Electron Spin Echo Envelope Modulation Spectroscopy Reveals and Distinguishes Equatorial and Axial Nitrogen Ligands Bound to VO^{2+}

Russell LoBrutto,*,‡ Brent J. Hamstra,† Gerard J. Colpas,† Vincent L. Pecoraro,† and Wayne D. Frasch‡

Contribution from the Department of Chemistry, The University of Michigan, Ann Arbor, Michigan 48109-1055, and The Center for the Study of Early Events in Photosynthesis and Department of Plant Biology, Arizona State University, Tempe, Arizona 85287-1601

Received October 7, 1997

Abstract: ESEEM (electron spin echo envelope modulation) spectra of a series of vanadyl complexes have for the first time revealed the spectral features that arise from amine nitrogen donors trans to the vanadyl oxo moiety. The complexes [$VO(H_2O)$ada] (**1**) and [$VO(H_2O)$Hheida] (**2**) (H_2ada, *N*-(2-acetamido)iminodiacetic acid; H_3heida, *N*-(2-hydroxyethyl)iminodiacetic acid) have recently been synthesized and crystallographically characterized (Hamstra, B. J.; Houseman, A. L. P.; Colpas, G. J.; Kampf, J. W.; LoBrutto, R.; Frasch, W. D.; Pecoraro, V. L. *Inorg. Chem.* **1997,** *36*, 4866−4874). In each structure, the ligand is disposed so that the tertiary nitrogen is bound trans to the vanadyl oxo. In solution, the structural integrity of these compounds is maintained as observed by UV/vis and EPR spectroscopies. ESEEM spectra of **1**, **2**, and [$VO(H_2O)$nta]$^-$ (**3**) (H_3nta, nitrilotriacetic acid) reveal that the superhyperfine coupling constants for axial amines are ≅1.3 MHz as opposed to the ≅5.0 MHz superhyperfine couplings typically observed for equatorially coordinated amines. The data indicate that not only can axial nitrogen donors to VO^{2+} be detected, but they may also be distinguished from nitrogen donors in the equatorial plane of the vanadyl ion. The implications of this study with respect to understanding the coordination environment of VO^{2+} in the vanadyl-substituted chloroplast F_1-ATPase (CF_1) and the reduced, inactive form of vanadium bromoperoxidase (VBrPO) are discussed.

Introduction

ESEEM (electron spin echo envelope modulation) spectroscopy is especially useful for the identification of nitrogen ligands coordinated to vanadium(IV) ions.[1] The weak superhyperfine couplings from equatorially coordinating nitrogen donors, not resolved in the CW EPR experiment, are easily observed through the use of ESEEM. Furthermore, the couplings observed can distinguish the types of nitrogen donors present, since the couplings to equatorial amine donors (lysine)[2,3] are significantly weaker than those from equatorial imidazole donors (histidine).[4,5]

The vanadyl ion has been probed by pulsed EPR techniques both in naturally occurring vanadoproteins and in vanadyl-substituted systems. A wide variety of vanadyl-substituted proteins have been studied by ESEEM spectroscopy, including pyruvate kinase,[2] *S*-adenosylmethionine synthetase,[3] D-xylose isomerase,[5] apoferritin,[4] lactoferrin and transferrin,[6] and chloroplast F_1-ATPase (CF_1).[7,8] In addition, the reduced form of the vanadium bromoperoxidase (VBrPO) from *Ascophyllum nodosum* has been examined using ESEEM spectroscopy.[9] We are particularly interested in CF_1 and VBrPO.

The chloroplast F_1-ATPase is the extrinsic membrane protein complex that, in association with the intrinsic membrane complex F_0, couples the proton motive force generated by the light reactions of photosynthesis to synthesize ATP. Closely related F_1-ATPases are found in mitochondria and bacteria. In the crystal structure of the F_1-ATPase from bovine mitochondria,[10] there are six sites for the binding of Mg(II) nucleotides, of which three are catalytic. The only protein-based metal ligand at either the catalytic or the noncatalytic sites is the hydroxyl group of threonine in the highly conserved phosphate-binding loop motif. Magnesium is an essential cofactor for this enzyme, and evidence strongly suggests that changes of the metal ligands during the course of the catalytic reaction are of critical importance for the enzyme to synthesize and dissociate ATP from the enzyme in the presence of an unfavorable chemical gradient of ATP to ADP and phosphate.[11] This nonequilibrium chemical gradient of ATP, which is maintained by the F_1F_0 complex, serves as the energy source for many biological processes. Information about the types of groups that

* To whom correspondence should be addressed.
† The University of Michigan.
‡ Arizona State University.

(1) Eaton, S. S.; Eaton, G. R. In *Vanadium in Biological Systems*; Chasteen, N. D., Ed.; Kluwer Academic Publishers: Dordrecht, The Netherlands, 1990; pp 199−222.
(2) Tipton, P. A.; McCracken, J.; Cornelius, J. B.; Peisach, J. *Biochemistry* **1989**, *28*, 5720−5728.
(3) Zhang, C.; Markham, G. D.; LoBrutto, R. *Biochemistry* **1993**, *32*, 9866−9873.
(4) Hanna, P. M.; Chasteen, N. D.; Rottman, G. A.; Aisen, P. *Biochemistry* **1991**, *30*, 9210−9216.
(5) Dikanov, S. A.; Tyryshkin, A. M.; Hüttermann, J.; Bogumil, R.; Witzel, H. *J. Am. Chem. Soc.* **1995**, *117*, 4976−4986.
(6) Eaton, S. S.; Dubach, J.; More, K. M.; Eaton, G. R.; Thurman, G.; Ambruso, D. R. *J. Biol. Chem.* **1989**, *264*, 4776−4781.
(7) (a) Houseman, A. L. P.; Morgan, L.; LoBrutto, R.; Frasch, W. D. *Biochemistry* **1994**, *33*, 4910−4917. (b) Houseman, A. L. P., LoBrutto, R., & Frasch, W. D. *Biochemistry* **1994,** *33*, 10000−10006.
(8) Houseman, A. L. P.; LoBrutto, R.; Frasch, W. D. *Biochemistry* **1995**, *34*, 3277−3285.
(9) de Boer, E.; Keijzers, C. P.; Klaassen, A. A. K.; Reijerse, E. J.; Collison, D.; Garner, C. D.; Wever, R. *FEBS Lett.* **1988**, *235*, 93−97.
(10) Abrahams, J. P.; Leslie, A. G. W.; Lutter, R.; Walker, J. E. *Nature* **1994**, *370*, 621−628.
(11) Weber, J.; Senior, A. E. *Biochim. Biophys. Acta* **1997**, *1319*, 19−58.

S0002-7863(97)03517-8 CCC: $15.00
Published on Web 04/28/1998

serve as metal ligands to the protein and how the ligands change upon activation of the F_1-ATPase has been obtained recently by examining the ^{51}V hyperfine parameters of the EPR spectra from vanadyl bound at specific Mg(II)-binding sites.[7,8]

Results obtained from EPR/ESEEM studies of vanadyl-substituted spinach chloroplast CF_1 suggest the presence of a coupled nitrogen nucleus with highly atypical properties, including ESEEM frequencies that lie entirely below 5.0 MHz.[8] Examination of the recently determined X-ray structure of the bovine heart enzyme[10] has led to identification of a lysine residue which is well within reach of the divalent cation (Mg^{2+} in the native enzyme). This lysine is an obvious potential ligand, and the preliminary ESEEM data hint that it may be an axial ligand to VO^{2+}.

The vanadium haloperoxidases were the first enzymes that were shown to have an essential requirement for vanadium.[12] The enzymes catalyze the oxidation of halides using hydrogen peroxide. Recently, the X-ray structure of an azide-inhibited V(V) enzyme has appeared.[13] The only protein-derived ligand is a coordinated histidine imidazole. Another imidazole that may be an acid/base catalyst is located near the vanadium ion. When the enzyme is reduced by one electron, it becomes catalytically inactive and there are distinct changes in the vanadium coordination sphere.[14]

The ESEEM study of the VBrPO is one of the earliest reports of pulsed EPR measurements on vanadyl in a protein.[9] The spectra shown therein have not been fully interpreted, and contain some modulation frequencies which are typical of equatorially coordinating nitrogen, and others which are not necessarily typical. This, combined with mechanistic considerations, raises the possibility of an additional nitrogen ligand to VO^{2+} that is trans to the vanadyl oxygen.

In the present work, we have undertaken a pulsed EPR study of a series of vanadyl aminocarboxylate complexes. These complement our crystallographic, UV/vis, and continuous wave EPR spectroscopic studies,[15] in conjunction with our interests in CF_1 and VBrPO. The ligands used are derivatives of iminodiacetic acid (Figure 1), and include a large number of ligand types that are electronically similar to potential donors to vanadium(IV) in biological systems. The complexes formed are stable in aqueous solution and are readily characterized structurally. These complexes are excellent spectroscopic models for the modulation of ESEEM spectra due to nitrogen ligation to vanadium(IV). Our results indicate that ESEEM spectroscopy of vanadium(IV)-substituted biological systems is a more powerful tool than has been previously reported, since not only can the types of nitrogen donors to vanadium be distinguished, but their relative orientations with respect to the vanadyl oxygen can be resolved as well. On the basis of this observation, we propose the presence of an axially bound lysine nitrogen ligand in CF_1 and we consider the possibility of an axial nitrogen ligand, in addition to the observed equatorial histidine ligand, in reduced VBrPO.[9]

Materials and Methods

The following abbreviations are used throughout the text: H_3nta, nitrilotriacetic acid; H_3heida, *N*-(2-hydroxyethyl)iminodiacetic acid; H_2-ada, *N*-(2-acetamido)iminodiacetic acid; CW EPR, continuous wave electron paramagnetic resonance. H_3nta and H_2ada were purchased from Aldrich Chemical Co. H_3heida was purchased from TCI.

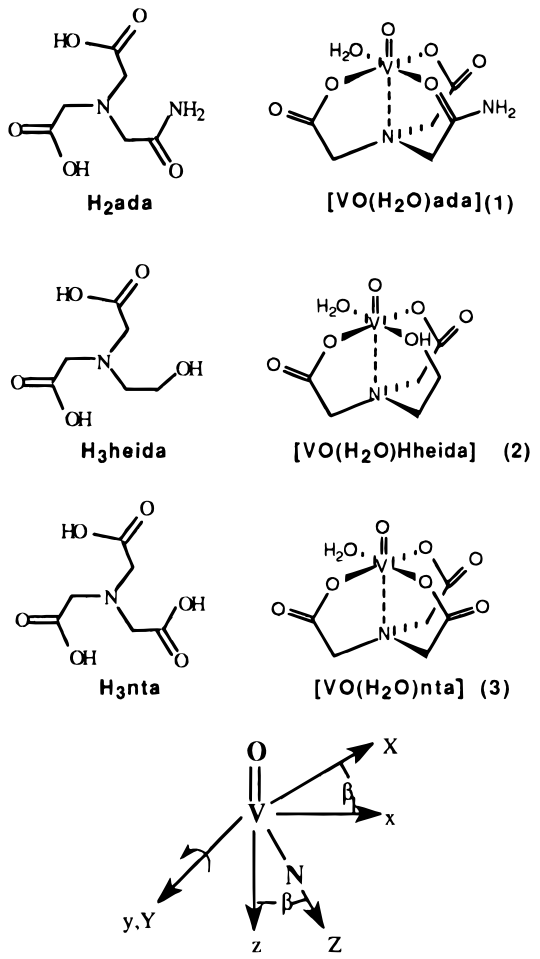

Figure 1. Ligand compounds used in this study and their complexes with VO(IV). The bottom diagram indicates the definition of the Euler angle β, which is varied in the simulations. The *xyz* system is the molecular (**g** tensor) reference frame, and the *XYZ* system represents the principal axes of the nuclear hyperfine or quadrupolar coupling tensor.

The samples used in ESEEM measurements were 1 mM solutions of $[VO(H_2O)ada]$, $[VO(H_2O)Hheida]$, or $[VO(H_2O)nta]^-$ in 50% (v/v) water/glycerol solution, at approximately pH 4.5 (Figure 1). Glycerol acts to form a good glass upon freezing, preventing spin aggregation that would otherwise shorten phase memory and reduce spectral resolution in the frequency domain. CW EPR spectra of all samples indicated the presence of a mixture of two species.[15] In each case the differences in the ^{51}V $A_{||}$ values were consistent with an equilibrium between a water and a carboxylate ligand.[16]

ESEEM Measurements. ESEEM spectra were obtained on a lab-built pulsed spectrometer, with a microwave bridge of standard design. For the purposes of the present study, the bridge was operated at 8.8−9.0 GHz. Pulse timing was generated by Stanford Research Systems DG535 digital delay generators, which were controlled by a Macintosh IIci computer, using National Instruments A/D and GPIB control hardware and the National Instruments LabView software package. This arrangement is similar in design to that described by Sturgeon et al.[17] The instrument employed a 50 W (nominal) pulsed traveling wave tube amplifier, and a one-loop, two-gap resonator[18] made of copper foil which was mounted on the "hourglass" quartz sample tube holder of an APD Cryogenics LTR liquid helium flow cryostat. The cryostat's

(12) Butler, A.; Walker, J. V. *Chem. Rev.* **1993**, *93*, 1937−1944.
(13) Messerschmidt, A.; Wever, R. *Proc. Natl. Acad. Sci. U.S.A.* **1996**, *93*, 392−396.
(14) Arber, J. M.; de Boer, E.; Garner, C. D.; Hasnain, S. S.; Wever, R. *Biochemistry* **1989**, *28*, 7968−7973.
(15) Hamstra, B. J.; Houseman, A. L. P.; Colpas, G. J.; Kampf, J. W.; LoBrutto, R.; Frasch, W. D.; Pecoraro, V. L. *Inorg. Chem.* **1997**, *36*, 4866−4874.
(16) Chasteen, N. D. In *Biological Magnetic Resonance*; Berliner, L. J., Reuben, J., Eds.; Plenum Press: New York, 1981; Vol. 3, pp 53−119.
(17) Sturgeon, B. E.; Britt, R. D. *Rev. Sci. Instrum.* **1992,** *63(4)*, 2187−2192.
(18) Froncisz, W.; Hyde, J. S. *J. Magn. Reson.* **1982**, *47*, 515−521.

quartz dewar insert was enclosed in a cylindrical brass shield which was coupled to an X-band waveguide via an oversized iris. Sample tubes were approximately 4.1 mm o.d. × 3.0 mm i.d.

The spectra shown herein were obtained exclusively from the "stimulated echo" sequence[19] of three $\pi/2$ pulses, each 18−20 ns in duration. Temperatures of 25−30 K and a pulse repetition rate of 1000 Hz were employed. Unwanted echoes were removed from the time-domain spectra by use of the standard, four-part phase cycle.[20] Spectra consisted of 1024 points over a time range of 0−10 μs, with each point typically being the sum of about 1000 individual echoes. Spin echo decay functions were fitted to fourth-order polynomials, which were then subtracted from time-domain ESEEM spectra. The residual modulation data were then apodized using a sine bell function to remove edge artifacts due to truncation of the data set, and Fourier transformed. Frequency-domain spectra were displayed in modulus form.

Numerical simulations of ESEEM spectra were performed using a program generously provided by Drs. A. M. Tyryshkin and S. A. Dikanov. The program, which performs full diagonalization of the spin Hamiltonian, allows for resolved hyperfine structure in the EPR spectrum, and calculates appropriate angle selection for a given experimental magnetic field. ESEEM due to superhyperfine couplings to nuclei with any nonzero spin can be simulated, and hyperfine, superhyperfine, and nuclear quadrupole coupling tensors can be rotated arbitrarily with respect to the **g** tensor principal axes.

Assignment of Modulation Frequencies. To aid in designating ^{14}N nuclear transition frequencies, we have adopted the notation used by Dikanov et al. in a study of VO^{2+} in D-xylose isomerase.[5] The two hyperfine manifolds are designated by "+" and "−" subscripts. The subscripts "sq" and "dq" refer to nuclear transitions of the type $\Delta m_I = \pm 1$ and $\Delta m_I = \pm 2$, respectively, and the superscripts "(1)" and "(2)" distinguish the two $\Delta m_I = \pm 1$ transitions within a given manifold.

Detailed measurements of magnetic-field dependencies of modulation frequencies have been used in assigning those frequencies to specific nuclear transitions. Increasing the magnetic field shifts the ν_+ frequencies upward and the ν_- frequencies downward. The rate of shift is proportional to the nuclear Zeeman frequency for the sq transitions, and to twice that frequency for dq transitions.

Analysis of ^{14}N ESEEM spectra is simplified if the hyperfine and externally applied magnetic fields approximately cancel at the nucleus for one value of the electron spin quantum number, m_S. The effective magnetic field experienced by a nucleus coupled to a single electron is the vector sum of these two fields. Let $\nu_{ef\pm}$ be the transition energies, expressed as frequencies, of the coupled nucleus for the two values of m_S. Then, $\nu_{ef\pm} = |\nu_L \pm |A_0|/2|$, where ν_L is the nuclear Larmor frequency at the applied laboratory field and $|A_0|$ is the magnitude of the isotropic hyperfine coupling, which is assumed to dominate. Let $K = e^2Qq/4h$, where e^2Qq/h is the standard nuclear quadrupole coupling constant, and define the asymmetry parameter $\eta = |q_{YY} - q_{XX}|/q_{ZZ}$, where q_{ii} $(i = X, Y, Z)$ are the principal values of the electric field gradient tensor. If $\nu_{ef}/K < 1$ for a given manifold, then one observes modulations near the pure NQR transition frequencies from that manifold:[21]

$$\nu_+ = K(3 + \eta), \quad \nu_- = K(3 - \eta), \quad \nu_o = 2K\eta \qquad (1)$$

The subscripts "+", "−", and "o" in eq 1 refer to different nuclear quadrupole transitions in the *same* manifold (i.e., for a single electron spin state), and should not be confused with the designations of + and − manifolds described above.

In the manifold where $\nu_{ef}/K > 1$, the anisotropy of the two ν_{sq+} transitions often causes them to be broadened beyond the limit of detectability. The ν_{dq+} transition, however, remains sharp and is easily observed in most cases.

(19) (a) Mims, W. B. *Phys. Rev.* **1972**, *B5*, 2409−2419. (b) Mims, W. B. *Phys. Rev.* **1972**, *B6*, 3543−3545.

(20) Fauth, J.-M.; Schweiger, A.; Braunschweiler, L.; Forrer, J.; Ernst, R. R. *J. Magn. Reson.* **1986**, *66* 74−85.

(21) Dikanov, S. A.; Tsvetkov, Yu. D. *Electron Spin Echo Envelope Modulation (ESEEM) Spectroscopy*; CRC Press: Boca Raton, FL, 1992; p 188.

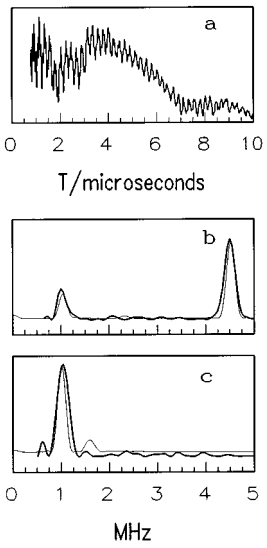

Figure 2. (a) Time-domain, stimulated echo ESEEM spectrum of [VO(H$_2$O)ada], obtained from the $m_I = +5/2_\perp$ EPR transition. Experimental conditions used: $\nu_e = 9.0198$ GHz; $B_o = 343.7$ mT; $T = 28$ K; $\tau = 190$ ns. (b) Frequency-domain ESEEM spectrum of [VO(H$_2$O)ada] (heavy line), obtained by Fourier transformation of (a). The lighter line shows the simulated spectrum. Simulation parameters: $g_{xx} = g_{yy} = 1.980$, $g_{zz} = 1.938$; ^{51}V hyperfine coupling; $A_{XX} = A_{YY} = 193.5$ MHz, $A_{ZZ} = 527$ MHz, Euler angles $\alpha = \gamma = 0°$, $\beta = 12°$; ^{14}N superhyperfine coupling, $A_{XX} = A_{YY} = 0.85$ MHz, $A_{ZZ} = 2.26$ MHz ($A_{iso} = 1.32$ MHz), Euler angles $\alpha = \gamma = 0°$, $\beta = 8°$; ^{14}N quadrupole coupling, $e^2Qq/h = 2.40$ MHz, $\eta = 0.86$, Euler angles $\alpha = \gamma = 0°$, $\beta = 12°$. (c) Frequency-domain, stimulated echo ESEEM spectrum of [VO(H$_2$O)ada] (heavy line), obtained from the $m_I = -7/2_{||}$ EPR transition. Experimental conditions used: $\nu_e = 8.9329$ GHz; $B_o = 264.0$ mT; $T = 27$ K; $\tau = 190$ ns. The lighter line shows the simulated spectrum. Simulation parameters for (c) are the same as for (b).

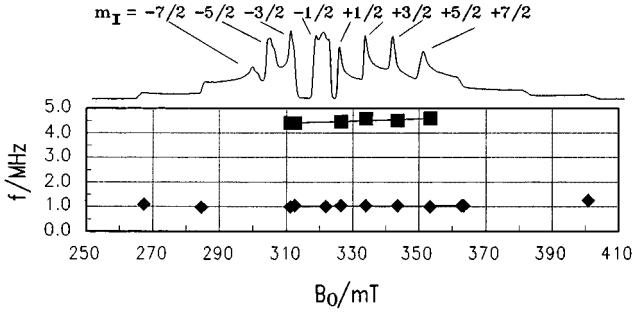

Figure 3. Magnetic field dependence of the stimulated echo ESEEM spectrum of [VO(H$_2$O)ada]. The spin echo-detected EPR spectrum is shown at the top of the graph for reference. The m_I values corresponding to each perpendicular feature in the spectrum are indicated.

Results

[VO(H$_2$O)ada]. Stimulated-echo ESEEM spectra of the [VO(H$_2$O)ada] complex were obtained at external magnetic fields corresponding to parallel and perpendicular orientations of the V═O axis with respect to the field direction. At perpendicular orientations (Figure 2a,b), modulations were observed at about 1.0 and 4.5 MHz, while only the former frequency was evident at fields corresponding to the parallel orientation (Figure 2c).

Shifts in the modulation frequency near 4.5 MHz as a function of laboratory magnetic field (Figure 3) were detectable even over the relatively narrow field range occupied by the "perpendicular" features of the CW spectrum. This peak shifts at twice the rate calculated from the Larmor frequency of ^{14}N,

and it is therefore assigned to the higher-frequency $\Delta m_I = \pm 2$ transition, labeled ν_{dq+}. No shift of the 1.0 MHz feature vs magnetic field was detectable against the background of scatter in the measured frequencies (Figure 3).

Analysis of EPR and ESEEM data was complicated by the presence of two major components in the EPR spectrum, in roughly equal proportions, as described in detail elsewhere.[15] Both components were simulated using the program QPOWA,[22] and the two resulting values of the parallel component of the ^{51}V hyperfine coupling parameter, $A_{||}$, were 527 and 535 MHz. The difference between these two numbers is consistent with an equilibrium involving exchange of a carboxylate and a water ligand at an equatorial site, according to data compiled by Chasteen.[16] The two species were not resolved in the spin echo-induced EPR spectra that were used for selection of EPR features upon which the ESEEM measurements were made (Figure 3). Thus, while both species would have contributed significantly to the spin echo amplitude, it is not clear whether one species or both contributed to the ^{14}N spin echo modulation trace shown in Figure 2a. The crystallographic analysis of [VO(H_2O)ada] shows two carboxylates and the amide carbonyl of the ligand coordinating the metal cation equatorially, forcing axial coordination of the tertiary amine.[15] Since this configuration would necessarily correspond to a smaller $A_{||}$ value than would a one-carboxylate, one-carbonyl, two-water equatorial set, it is reasonable to assume that at least the species with $A_{||} = 527$ MHz is contributing to the spin echo modulations. In principle, the other species could contribute identically, differently, or not at all (cf. the Discussion).

Initial ESEEM simulations (Figure 2) were performed under the assumption that the magnetic field was fixed on the $+5/2_{\perp}$ feature of the EPR absorption. The procedure used to fit the data was as follows. The **g** and ^{51}V **A** tensors were obtained from simulation of the CW EPR spectral component with the weaker hyperfine coupling. The values used were $g_{xx} = g_{yy} = 1.982$, $g_{zz} = 1.938$, $A_{XX} = A_{YY} = 193.5$ MHz, and $A_{ZZ} = 527$ MHz. The Euler angles, α, β, and γ, relating these two tensors' orientations were initially set to zero. The V−N bond length was fixed at 2.3 Å, the value obtained from X-ray crystallographic measurements on the complexes. Using a point-dipole approximation, this distance was translated into an absolute value of 0.47 MHz for the ^{14}N dipolar hyperfine coupling parameter, $T_{\perp}$. For an axially symmetric hyperfine interaction, the principal values of the zero-trace dipolar hyperfine coupling tensor are given by $(T_{\perp}, T_{\perp}, -2T_{\perp})$. The ^{14}N superhyperfine coupling was initially assumed to have axial symmetry, and it was not necessary to relax this condition in order to obtain acceptable simulations. With the quadrupolar asymmetry parameter η initially set equal to 1.0, the parameters A_0 (the isotropic component of the^{14}N superhyperfine coupling) and e^2Qq/h were adjusted until the two simulated modulation frequencies matched those in the experimental spectrum. Changes in A_0 had a greater effect on the higher-frequency feature, but still affected the lower-frequency feature detectably; the opposite was true for e^2Qq/h. The initial value of η was chosen because it gives NQR frequencies $K(3 - \eta)$ and $2K\eta$ that are equal. The result will be coincident ESEEM frequencies if the hyperfine and laboratory fields cancel exactly. This is consistent with the observation of only one frequency from the negative manifold. In final adjustments to refine the fit to the data, η was reduced to 0.86.

Once the frequencies were optimized by adjusting A_0 and e^2Qq/h, it was found that the simulated 4.5 MHz feature was much less intense than that at 1.0 MHz, contrary to the data. Adjustments to η and to Euler angles of the superhyperfine and quadrupolar tensors did not produce the magnitude of amplitude shifts needed to fit the data. It was found, though, that a small rotation through the angle β of the ^{51}V hyperfine tensor permitted straightforward correction of the amplitudes. Accompanying line shape changes were then compensated by minor adjustments of the angles β of the ^{14}N nuclear quadrupole and hyperfine tensors. The effects of varying the angles α and γ were not explored. The final values of the parameters used to achieve the fits shown in Figure 2 are as follows: **g** and **A** tensor principal values as given above; ^{51}V hyperfine coupling Euler angles, $\alpha = \gamma = 0°$, $\beta = 12°$; ^{14}N superhyperfine coupling, $A_{XX} = A_{YY} = 0.85$ MHz, $A_{ZZ} = 2.26$ MHz ($A_0 = 1.32$ MHz), Euler angles $\alpha = \gamma = 0°$, $\beta = 8°$; ^{14}N quadrupole coupling, $e^2Qq/h = 2.40$ MHz, $\eta = 0.86$, Euler angles $\alpha = \gamma = 0°$, $\beta = 12°$. The Euler angles are expressed using the principal axes of **g** as a reference frame.

The optimized parameters give ν_{ef-} near 0.40 MHz at typical fields, and since the parameter $K = e^2Qq/4 = 0.60$ MHz, it is found that ν_{ef}/K is significantly less than 1.0 in the negative hyperfine manifold. It follows that one should expect to observe transitions near the pure NQR frequencies, whose values are $[K(3 + \eta), K(3 - \eta), 2K\eta] = [2.3, 1.3, 1.0]$ MHz. In the simulation, as in the experimental spectrum, only a single peak is observed in the range below 2 MHz. This must occur either because one of the ν_{sq-} transitions is too broad and weak to observe, or because both transitions of this type are near 1.0 MHz and are not resolved.

The simulations confirm that the ν_{dq-} modulation, near 2.3 MHz, can be expected to be quite weak under the conditions used (cf. the Discussion). Thus, its absence from the experimental spectra, where the signal-to-noise ratio is limited, does not contradict the above assignment of transitions. As expected, the $\nu^{(1)}_{sq+}$ and $\nu^{(2)}_{sq+}$ transitions are not observed, because they are far more anisotropic than ν_{dq+}.[23] It is noted that the pulse delay time τ was varied over a wide range to ensure that no significant modulation frequencies went undetected due to suppression effects in the three-pulse experiment.[19]

[VO(H_2O)nta]$^-$. The results of orientation-dependent ESEEM measurements on the [VO(H_2O)nta]$^-$ complex (Figure 4) were nearly identical to those shown for the [VO(H_2O)ada] complex. At the $+5/2_{\perp}$ field setting (Figure 4a), a small upward shift in the frequency of the feature near 1.0 MHz was observed, together with slight broadening. At the $-7/2_{||}$ position, the "1.0 MHz" peak was shifted slightly downward (Figure 4b). These differences were accounted for in simulations, partly by shifts in angle selection due to minor changes in the CW EPR parameters of the complexes, and partly by a slight change in the ^{14}N superhyperfine coupling tensor. The magnetic field dependencies of the observable transitions (Figure 5) matched well those of [VO(H_2O)ada].

[VO(H_2O)Hheida]. The ESEEM characteristics of the [VO(H_2O)Hheida] complex were also quite similar to those of [VO(H_2O)ada], with two very minor differences (Figure 6). First, the two main features (near 1.0 and 4.5 MHz at "perpendicular" magnetic field settings) were more nearly equal in amplitude. Second, the [VO(H_2O)Hheida] spectra show better evidence of a weak component between 2.0 and 2.5 MHz (probably the ν_{dq-}

(22) (a) Nilges, M. J. Ph.D. Thesis, University of Illinois, Urbana, IL, 1979. (b) Belford, R. L.; Nilges, M. J. *Computer Simulation Of Powder Spectra*, EPR Symposium, 21st Rocky Mountain Conference, Denver, CO, August 1979. (c) Maurice, A. M. Ph.D. Thesis, University of Illinois, Urbana, IL, 1980.

(23) Mims, W. B.; Peisach, J. *J. Chem. Phys.* **1978**, *69*, 4921−4930.

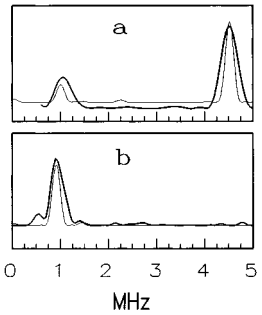

Figure 4. (a) Stimulated echo ESEEM spectrum of $[VO(H_2O)nta]^-$ (heavy line), obtained from the $m_I = +5/2_\perp$ EPR transition. Experimental conditions used: $\nu_e = 9.0201$ GHz; $B_o = 342.7$ mT; $T = 28$ K; $\tau = 190$ ns. The lighter line shows the simulated spectrum. Simulation parameters: $g_{xx} = g_{yy} = 1.979$, $g_{zz} = 1.939$; ^{51}V hyperfine coupling; $A_{XX} = A_{YY} = 68.9$ G, $A_{ZZ} = 187$ G, Euler angles $\alpha = \gamma = 0°$, $\beta = 12°$, ^{14}N superhyperfine coupling, $A_{XX} = A_{YY} = 0.88$ MHz, $A_{ZZ} = 2.29$ MHz ($A_{iso} = 1.35$ MHz), Euler angles $\alpha = \gamma = 0°$, $\beta = 8°$; ^{14}N quadrupole coupling, $e^2Qq/h = 2.40$ MHz, $\eta = 0.86$, Euler angles $\alpha = \gamma = 0°$, $\beta = 12°$. (b) Stimulated echo ESEEM spectrum of $[VO(H_2O)nta]^-$ (heavy line), obtained from the $m_I = -7/2_{||}$ EPR transition. Experimental conditions used: $\nu_e = 8.9329$ GHz; $B_o = 264.0$ mT; $T = 27$ K; $\tau = 290$ ns. The lighter line shows the simulated spectrum. Simulation parameters for (b) are the same as for (a).

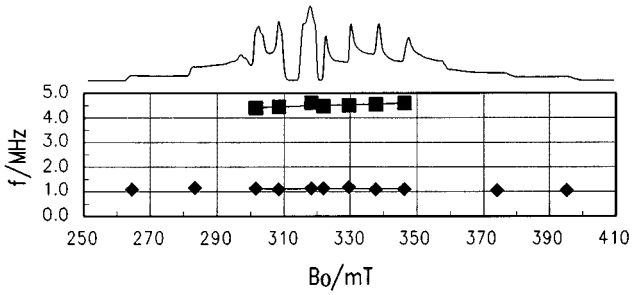

Figure 5. Magnetic field dependence of the stimulated echo ESEEM spectrum of $[VO(H_2O)nta]^-$. The spin echo-detected EPR spectrum is shown at the top of the graph for reference.

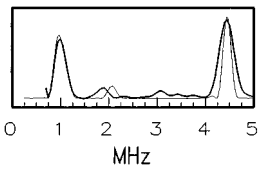

Figure 6. Stimulated echo ESEEM spectrum of $[VO(H_2O)Hheida]$ (heavy line) obtained from the $m_I = +1/2_\perp$ EPR transition. Experimental conditions used: $\nu_e = 8.9204$ GHz; $B_o = 326.0$ mT; $T = 30$ K; $\tau = 190$ ns. The lighter line shows the simulated spectrum. Simulation parameters: $g_{xx} = g_{yy} = 1.979$; $g_{zz} = 1.937$; ^{51}V hyperfine coupling, $A_{XX} = A_{YY} = 70.0$ G, $A_{ZZ} = 189$ G, Euler angles $\alpha = \gamma = 0°$, $\beta = 12°$; ^{14}N superhyperfine coupling, $A_{XX} = A_{YY} = 0.92$ MHz, $A_{ZZ} = 2.33$ MHz ($A_{iso} = 1.39$ MHz), Euler angles $\alpha = \gamma = 0°$, $\beta = 8°$; ^{14}N quadrupole coupling, $e^2Qq/h = 2.10$ MHz, $\eta = 0.90$, Euler angles $\alpha = \gamma = 0°$, $\beta = 12°$.

transition) whose presence was predicted both from first-order analysis and from full numerical simulations. These differences were simulated as small shifts in the ^{14}N nuclear quadrupolar parameters: e^2Qq/h was reduced to 2.10 MHz, and η was increased to 0.9. While achieving a precise match in relative amplitudes proved to be difficult, the same set of ^{14}N superhyperfine coupling parameters as was used for $[VO(H_2O)ada]$ was adequate to generate the major features of the $[VO(H_2O)$-Hheida] spectrum at their correct frequencies. The variation of the two main modulation frequencies versus magnetic field (not shown) was also the same as for $[VO(H_2O)ada]$.

Discussion

Vanadyl Complexes with Model Ligands. Simulated ESEEM data for all three compounds fit the experimental data well upon assumption of the following approximate ^{14}N superhyperfine coupling parameters: $A_{xx} = A_{yy} = 0.9$ MHz; $A_{zz} = 2.3$ MHz ($A_0 = 1.3$ MHz). This coupling is far too small to be attributed to an equatorially coordinating amino nitrogen, for which A_0 would be near 5 MHz.[3] The unpaired electron on the VO^{2+} cation is mainly localized in the d_{xy} orbital of vanadium; the lobes of that orbital lie in or near the plane defined by the equatorial ligands. Therefore, a nonzero spin nucleus positioned trans to the vanadyl oxo should have a much smaller A_0 than the same nucleus at the same distance from the vanadium but cis to the oxo. Furthermore, the distances are not equivalent. The crystal structures of $[VO(H_2O)ada]$ and $[VO(H_2O)Hheida]$ indicate equatorial V−N bond lengths near 2.0 Å, but axial V−N bonds which are 2.3 Å long.[15] Because the unpaired electron is in or near the equatorial plane, the use of a point dipole approximation to translate the V−N distance into a value for the dipolar parameter $T_\perp$ for use in the simulation is reasonable. Acceptable theoretical fits to the data were obtained without changing the assumed V−N bond length. The fits did not improve when, at the end of the simulation process, this distance was allowed to vary.

The simulated spectra generally matched the experimental data well. Imperfections in the simulations may arise from the mixing of ESEEM spectra from two different species with different ^{51}V hyperfine couplings. In such cases, the ^{14}N coupling parameters may be nearly unchanged between species, but the contributions to the ESEEM spectra at a given field setting may be different. This is because the set of molecular orientations selected at a given dc field setting will differ for the two species. Since the variation in the ^{51}V (and **g**) tensors between species is small, the effects on the ESEEM spectrum should be relatively minor. The consistency of the ESEEM data generally supports this view. As noted above, however, significant scatter was observed in the frequency of the feature near 1 MHz, as a function of magnetic field. The scatter was large enough to obscure any clear trend in the field dependence, and it is likely attributable to a combination of differential angle selection between species, and a limited signal-to-noise ratio in the wings of the EPR spectrum.

The above explanation assumes that the two species present in each sample contribute roughly equally to modulation of the spin echo amplitude. The properties of the CW EPR spectra of the ESEEM samples support this assumption. As indicated in the Results, the difference between the two $A_{||}$ values in each CW spectrum corresponds to that expected for an equilibrium between a single carboxylate and water ligand. If one or more of the other carboxylates were to exchange with solvent in significant proportions, additional species would be observed, with still larger values of $A_{||}$. With all but one of the initial equatorial coordinating groups in place, axial nitrogen coordination is very likely for the 535 MHz species as well. The detailed EPR and crystallographic analyses of these complexes that were reported recently confirm the identities of the two major species in each solution.[15]

Rotation of $\beta(^{51}V)$ through a small angle away from zero tacitly assumes that the axes of the metal hyperfine tensor are slightly skewed with respect to the molecular framework. This is not an unusual occurrence in general, and in the particular case of the VO/model ligand complexes, it meshes remarkably well with the crystallographic data. The crystal structures of the $[VO(H_2O)ada]$ and $[VO(H_2O)Hheida]$ complexes reveal that

the O═V−N bond angles are 172.6° and 169.4°, respectively.[15] Thus, the deviations from linearity are similar to the proposed rotations of the ^{51}V tensor. The latter are naturally less precisely determined than the crystallographic angles, but the similarities in magnitudes of the angles are probably not coincidental. The isolated ligands have 3-fold symmetry (nta) or pseudo-3-fold symmetry (ada and heida). The "arms" of each compound attempt to coordinate an ion whose orbital structure in its equatorial plane is (initially) 4-fold symmetric. One would therefore expect some level of strain within the complex in order for the coordination to occur as it does in the crystal structure. This strain is probably responsible for pulling the amino nitrogen off the axis defined by the V═O bond, and for the rotation of the hyperfine coupling tensor of the metal with respect to that axis.

The compression of the O═V−N bond angle should also produce a small rotation of the ^{14}N superhyperfine tensor, and this feature is built into the parameters used to simulate the ESEEM spectrum. The rotation of the nuclear quadrupole tensor, rather than being a direct consequence of the off-axis positioning of the nitrogen, is more likely due to rotation of the 3-fold symmetry axis of the ligand itself (and therefore of the *z*-axis of the nuclear quadrupole tensor) away from the V═O direction. The strain on the complex described above could also generate asymmetry in the electric field gradient in the $x-y$ plane, and thus it is physically reasonable to expect a value of the asymmetry parameter η that is substantially larger than zero.

The ESEEM spectrum of the [$VO(H_2O)$Hheida] complex exhibited a feature in the 2−3 MHz range that was not present in spectra of the other complexes. This feature was typically very weak, and its apparent frequency may have been shifted by the effect of its interaction with spectral noise (note the broad, weak component near 2 MHz in Figure 6). In most spectra in which it did appear, however, its frequency and amplitude were close to those of the simulated ν_{dq-} peak.

The minimal amplitude of the ν_{dq-} peak was unexpected. It is best explained by considering the standard analysis of an ^{14}N coupling near "exact match" conditions. Such a coupling might typically be obtained from the noncoordinating nitrogen of an imidazole ring, whose other nitrogen coordinates a metal ion such as copper. In that case, there is significant through-bond transfer of electron spin to the remote nitrogen, imparting an isotropic hyperfine coupling of up to a few megahertz. At the same time, the separation of three bond lengths between the nitrogen and the metal produces anisotropic superhyperfine couplings of just a few tenths of a megahertz. A four-line ESEEM spectrum usually results, in which the three lowest frequencies approximate the zero-field NQR frequencies.

The present case differs from that just described due to the electronic structure of the VO^{2+} cation. Because the unpaired electron resides in the plane orthogonal to the V═O double bond, an axial ligand can approach the vanadium ion quite closely with only weak transfer of electron spin density to the ligand nucleus. Thus, instead of differing by an order of magnitude, the isotropic and anisotropic parts of the ^{14}N superhyperfine coupling are very nearly the same. The unusually large dipolar (anisotropic) component of the coupling may broaden the ν_{dq-} transition severely. To test this explanation, the best-fit parameter set for the [$VO(H_2O)$ada] complex (cf. the Results) was altered such that the parameter $T_\perp$ corresponded to a V−N distance of about 3.4 Å. This value was chosen because it yielded a more typical ratio of isotropic to anisotropic components of the coupling. As Figure 7 shows, the result (for the perpendicular orientation) is much closer to a standard four-line spectrum. The ν_{dq-} transition stands out plainly at 2.4 MHz. In addition, the two ν_{sq-} transitions are visible and partly resolved, and their frequencies add to give the ν_{dq-} frequency.

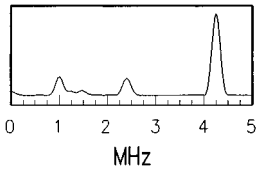

Figure 7. Simulation using the same parameters as in Figure 2a, except that the effective V−N distance is changed from 2.3 to 3.4 Å.

The question of how to identify an axially coordinating nitrogen in a vanadyl complex has been raised, directly or indirectly, in at least two other studies. An ENDOR study of bis(acetylacetonato)oxovanadium in chloroform/toluene, with dilute pyridine added, examined two alternative structures for the complex formed.[24] In one hypothetical structure, the two acetylacetonate moieties coordinated symmetrically, with four carbonyl oxygen equatorial ligands complemented by an axial pyridine nitrogen. In the other, the coordination was asymmetric, with pyridine cis to the vanadyl oxygen, and one of the acetylacetonate oxygens coordinating axially. It was suggested, on the basis of ^{1}H and ^{14}N ENDOR measurements, that pyridine was more likely cis to the oxo. A nitrogen hyperfine coupling near 6.5 MHz was obtained, but at the time, it was not clear whether an axially coordinating nitrogen could also give rise to such a coupling. On the basis of the present results, if the hyperfine coupling of a pyridine nitrogen ligand were reduced by the same ratio as that of an amino nitrogen upon switching from equatorial to axial coordination, the pyridine nitrogen's isotropic hyperfine coupling constant would be only about 1.8 MHz. Early ESEEM measurements on the same complex suggested a coupling constant in the 3−6 MHz range.[25] The present work confirms that those ENDOR and ESEEM results were indeed indicative of an asymmetric coordination scheme.

Chloroplast F_1-ATPase. The stimulated-echo ESEEM spectrum obtained from a mixed-state sample of VO^{2+}-substituted spinach chloroplast F_1-ATPase contains modulation frequencies within the same range as those from the model complexes described above. In a recent study, we reported a spectrum of VO^{2+} in this protein, obtained at 8.16 GHz, which exhibited modulations at about 1.0, 3.2, and 3.8 MHz.[8] It is possible to project the 3.8 MHz feature upward to the microwave frequency (and thus the magnetic field) used in the present model study, assuming that the data were to be obtained at the same effective *g* value, and that the 3.8 MHz modulation corresponds to a $\Delta m_I = \pm 2$ transition. The resulting frequency would be about 4.0 MHz, not far from the 4.5 MHz modulation reported here. Some differences are to be expected, if only because the magnitude and symmetry of the nuclear quadrupolar interaction are different for primary versus tertiary amines. The ATPase spectrum has not yet been thoroughly analyzed, in part because a more complete data set is needed. Nonetheless, the similarity between the protein and model spectra is suggestive of axial nitrogen coordination.

The CW EPR and ESEEM data complement the published crystal structure of CF_1. Combining these has led to development of a hypothetical model for the coordination of VO^{2+} bound to the catalytic site 3 in the latent state of the spinach enzyme (Figure 8). In this model, one carboxylate (aspartate or glutamate) and one hydroxyl side chain each coordinates

(24) Kirste, B.; van Willigen, H. *J. Phys. Chem.* **1982**, *86*, 2743−2749.
(25) Astashkin, A. V.; Dikanov, S. A.; Tsvetkov, Yu. D. *Zh. Struct. Khim.* **1985**, *26* (3), 53; *J. Struct. Chem.* **1985**, *26*, 363−368.

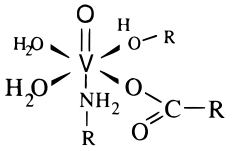

Figure 8. Proposed coordination scheme for vanadyl cation in the latent state of the chloroplast F_1-ATPase, site 3.

VO^{2+} equatorially, along with two water molecules. The axial ligand is the ϵ-amino nitrogen of a lysine residue.

Vanadium Bromoperoxidase. The ESEEM spectrum of the reduced, inactive form of vanadium-dependent bromoperoxidase was reported by de Boer et al.[9] Modulation frequencies of 3.1, 4.2, 5.3, and 8.1 MHz were observed at a field setting corresponding to a mixture of parallel and perpendicular orientations of the V═O axis with respect to the field direction, and at 3.0, 4.7, 5.3, and 8.6 MHz when the perpendicular orientation was selectively monitored. It is reasonable to suggest that, in each case, two of the observed components of the spectrum arise from the $\Delta m_I = \pm 2$ transitions of a histidine imidazole nitrogen coordinated in the equatorial plane of the vanadyl ion. The highest, plus either the second- or third-highest, frequency is the likely candidate in this case. Similar features have been observed in imidazole-ligated complexes by other investigators.[6]

The source of the lower-frequency components of the VBrPO spectrum is less clear. In the above-mentioned study, the ESEEM spectrum of the complex $[VO(meox)_2]$ (meox = anion of 2-methyl-8-quinolinol) was measured, and exhibited frequencies of 3.2, 4.8, 5.8, and 8.4 MHz at field settings corresponding to the analogous positions in the VBrPO EPR spectrum. In the crystal structure of $[VO(meox)_2]$, the two nitrogen donors to vanadium are equivalent and near the equatorial plane of the vanadyl ion (N−V−O(oxo) angle 99.5(5)^o), and the quinolinol oxygen donors are displaced farther from the equatorial plane away from the vanadyl oxo (O−V−O(oxo) angle 116.4(7)°), yielding what may be considered to be a distorted trigonal bipyramidal geometry.[26] In five-coordinate complexes such as $[VO(meox)_2]$ that contain bidentate ligands, there may be fluxional behavior in solution which gives rise to alternative coordination geometries. In this case it may be possible that one or more of the four frequencies observed for $[VO(meox)_2]$ arises from a nitrogen donor that is in a different environment from that observed in the crystal structure. Support for this assertion comes from analysis of ESEEM spectra of the complex [VO(salen)], which contains a similar set of donors to $[VO(meox)_2]$ and whose nitrogen donors are in similar positions relative to the vanadyl ion when compared to those in $[VO(meox)_2]$. [VO(salen)] yields an ESEEM spectrum that contains only modulation frequencies at 5.0, 5.7, and 9.0 MHz, and no frequencies near 3.0 MHz as are observed for $[VO(meox)_2]$.[9]

The data obtained in the present study for other model complexes suggest that the 3.0 MHz frequency in VBrPO may arise from a nitrogen donor significantly displaced from the equatorial plane of the vanadyl ion, if not in an axial position. Although none of the complexes in the present study yield spectra that closely match the features of the VBrPO ESEEM spectrum, close correlation between the different spectra might not be expected. This is because none of the complexes considered in this study contained imidazoles or other similar donors in the axial coordination position. It is not clear at this time exactly what effects axially coordinated donors of this type might have on the ESEEM spectra of vanadyl complexes. As mentioned above, a reduction in superhyperfine coupling for a pyridine donor comparable to that observed for the amine donors in this study would yield an isotropic hyperfine coupling constant of about 1.8 MHz. We are currently pursuing the synthesis and characterization of complexes which would allow us to answer this question with greater confidence.

We recently reported an analysis of the CW EPR data obtained for the reduced VBrPO,[15] using the additivity relationship as defined by Chasteen.[16] Our analysis, which took into account the various spectroscopic and crystallographic data known for VHPOs, suggested that the most likely set of equatorial ligands included one or two histidine imidazoles. If an additional imidazole donor is bound in an axial or near-axial position as the ESEEM data may indicate, then this would be in addition to those imidazole ligands whose presence is inferred as a result of the additivity calculations. The irreversible inactivation of VHPOs upon reduction may be a consequence of binding additional histidine(s) to vanadium(IV), perhaps by binding an essential acid/base catalyst (potentially His-101 in the VBrPO) and/or inducing significant structural changes that inhibit reoxidation to the active vanadium(V) form or inhibit steps in the catalytic cycle other than those requiring acid/base catalysis.[15]

Conclusion

We have measured and analyzed the ESEEM spectra of several complexes containing axially bound nitrogen ligands. These data indicate that ESEEM can be used not only to establish the presence and type of nitrogen ligands bound to vanadium, but to determine whether the relative position with respect to the vanadyl ion is equatorial or axial. This discovery is directly relevant to the interpretation of ESEEM spectra for vanadyl-substituted CF_1, and may also be relevant for understanding the active site structure and inactivation of reduced vanadium-dependent haloperoxidases. These studies pave the way for expanded use of ESEEM spectroscopy of the vanadyl ion as a probe of structure both in naturally occurring vanadoproteins and in systems where VO^{2+} is used as a spectroscopic surrogate for divalent ions such as Mg^{2+} and Ca^{2+} that are normally spectroscopically inaccessible.

Acknowledgment. The authors are grateful to Dr. Ralph Weber of Bruker Instruments, Inc., for his assistance in obtaining the spin echo-detected EPR spectra. Financial support from National Institutes of Health Grants GM50202 (to W.D.F.) and GM42703 (to V.L.P.) is gratefully acknowledged.

JA973517S

(26) Shiro, M.; Fernando, Q. *Anal. Chem.* **1971**, *43*, 1222−1230.